REPORT DOCUMENTATION PAGE

Form Approved
OMB No. 0704-0188

1. REPORT DATE *(DD-MM-YYYY)*	2. REPORT TYPE	3. DATES COVERED *(From - To)*
07/09/2005	Final	06/08/04-06/07/05

4. TITLE AND SUBTITLE
Diagnostic Testing And NIKE Experiments

5a. CONTRACT NUMBER
N00173-04-1-G905

5b. GRANT NUMBER

5c. PROGRAM ELEMENT NUMBER

6. AUTHOR(S)
R. Paul Drake
Eric C. Harding

5d. PROJECT NUMBER

5e. TASK NUMBER

5f. WORK UNIT NUMBER

7. PERFORMING ORGANIZATION NAME(S) AND ADDRESS(ES)
University of Michigan, Space Physics Research Laboratory, 2455 Hayward, Ann Arbor, MI 48105

8. PERFORMING ORGANIZATION REPORT NUMBER
N/A

9. SPONSORING/MONITORING AGENCY NAME(S) AND ADDRESS(ES)
Department of Navy, Department of Defense
Naval Research Laboratory
Laser Plasma Branch
Steven Obenschain, Branch Head
4555 Overlook Ave S.W., Washington DC 20375

10. SPONSOR/MONITOR'S ACRONYM(S)
NRL

11. SPONSOR/MONITOR'S REPORT NUMBER(S)
N/A

12. DISTRIBUTION/AVAILABILITY STATEMENT
No restrictions

13. SUPPLEMENTARY NOTES
None

14. ABSTRACT

Under this contract we have developed a Monte Carlo model of microchannel plate performance, made measurements for comparison with the model, and identified potential strategies for improving the performance of microchannel plates in analog imaging applications. This has prepared us to address the optimization of x-ray framing cameras for NRL applications and long-term possibilities for improvements in performance. In addition, we participated in work at NIKE and gained experience relevant to working in the NIKE environment.

15. SUBJECT TERMS
Laser plasma diagnostics, NIKE laser, microchannel plates

16. SECURITY CLASSIFICATION OF:			17. LIMITATION OF ABSTRACT	18. NUMBER OF PAGES	19a. NAME OF RESPONSIBLE PERSON
a. REPORT	b. ABSTRACT	c. THIS PAGE			R. Paul Drake
UU	UU	UU	None	13	19b. TELEPHONE NUMBER *(Include area code)* 734-763-4072

Final Report

Diagnostic Testing and NIKE Experiments

Principal Investigator:

R. Paul Drake,
University of Michigan

August 1, 2005

Award No. N00173-04-1-G905

ABSTRACT

Under this contract we have developed a Monte Carlo model of microchannel plate performance, made measurements for comparison with the model, and identified potential strategies for improving the performance of microchannel plates in analog imaging applications. This has prepared us to address the optimization of x-ray framing cameras for NRL applications and long-term possibilities for improvements in performance. In addition, we participated in work at NIKE and gained experience relevant to working in the NIKE environment.

1. INTRODUCTION

We have been training a graduate student, Eric Harding, in areas relevant to x-ray diagnostics of interest to NRL and to hydrodynamic experiments at NRL. In addition, both Eric and a number of additional contributors have worked to develop our x-ray-diagnostic characterization system and have made a number of measurements using it. During the past year, Eric has crossed the threshold from being in training regarding diagnostics using microchannel plates (MCPs) to doing independent research in this area. This led to some very informative measurements and to an explosion of modeling work. As a result, we can now evaluate diagnostics using MCPs with increased sophistication. We believe that our ability to analyze and model the behavior of MCPs for analog imaging applications now exceeds the previous state of the art (most previous work is dedicated to pulse-counting applications). This has prepared us to address the optimization of x-ray framing cameras for NRL applications and long-term possibilities for improvements in performance. Both Eric and another student spent time at NRL during 2004, helping with diagnostic development and becoming able to work in the NRL environment. In addition, Eric has completed coursework in high-energy-density physics and in compressible turbulence that prepare him to think about novel experiments.

2. FRAMING-CAMERA-RELATED RESEARCH

This section discusses key results related to framing camera improvement, related activity in our laboratory, and our participation at NRL.

A. Framing camera improvement: key results

It has been the point of view of the community using microchannel plates (MCPs) for analog imaging that the primary factor limiting the performance of these devices has been the quantum efficiency. Here, quantum efficiency is defined as the fraction of incident photons that produce signal in the detector. This point of view has been supported by a number of measurements reported in the literature **[1-5]** that seem to indicate a quantum efficiency in the range of 1 to 10%. In particular, this was the result that Carl Pawley obtained at NRL by statistically measuring the Detected Quantum Efficiency (DQE) of an MCP with a gold photocathode (created when "striplines" were laid down to allow gating of the plate). We discuss DQE further below, where we will see that a standard framing camera at present achieves a DQE that is far below the potential maximum value. The conclusion is that the noise introduced by framing cameras might be greatly reduced by improved design.

An important point is that a measurement seeking to determine an averaged quantum efficiency by statistical means must operate with a low photon flux, so that the Poisson statistics of the output is determined by the limited number of detected events. This led us to seek to measure single-photoelectron events, obtaining Fig. 1.

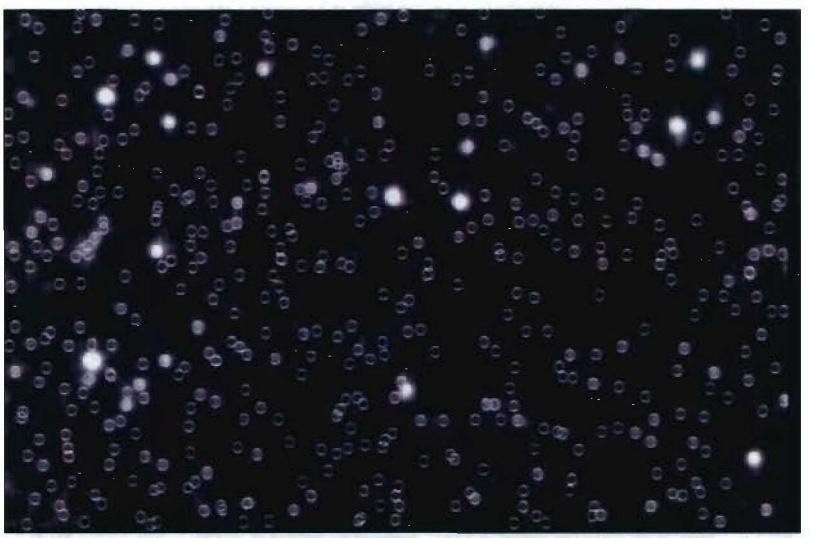

Figure 1. Single-photoelectron events detected with our x-ray system. The data have been processed using a star-finder program adapted by Eric Harding. This produced the circles on the plot, which are also present for the bright dots but do not show up on this display. The measurement used a 2 inch diameter MCP. It has a CsI photocathode coating to a depth of 1.5 pore diameters. The MCP properties were: pore diameter 10 μm, thickness of MCP 600 μm, bias angle 8 degrees, and applied voltage 1150 V. The x-ray properties were: energy 1.49 keV (Al Kα), 0.016 average incident photons entering each MCP pore, 500 events found, δG/G ~ 1.5, quantum efficiency 39%.

The first notable aspect of these data is that the brightness of the dots varies greatly. This corresponds to a variation in the gain from one event to the next. Statistically, the standard deviation of the intensity of the dots in this image, δG, is 1.5 times the average intensity, G. This is enough to overwhelm any statistical variation due to finite quantum efficiency. Indeed, through further analysis, discussed below, we have concluded that the quantum efficiency of clean CsI in this application should approach unity (for the CsI within the MCP pores). For framing-camera applications, the actual problem of optimizing the performance of MCPs becomes one of minimizing the total noise. This includes producing as many photoelectrons as feasible, but only with limits that do not create too much additional noise.

The observation of large gain variations in the sense seen in Fig. 1 led us to think further about DQE, discussed next, and then to build a Monte Carlo model of electron production in MCPs. We learned a great deal in the process. This has the effect of increasing the promise of using a grid to reflect photoelectrons from the surface down into the pores and of introducing new ideas including the use of MCPs with square channels. We explain this and other potential improvements after providing the relevant background.

B. Understanding DQE

The Detected Quantum Efficiency (*DQE*) is often used as a measure of instrument performance. *DQE* is defined by

$$DQE = \left(\frac{\sigma_i / n_i}{\sigma_o / n_o} \right)^2 , \qquad (1)$$

in which the average input signal is n_i, the standard deviation of the input is σ_i, the average output signal is n_o, and the standard deviation of the output is σ_o. The meaning of *DQE* can be seen by some simple calculations. The input, presumed to be photons here, involves an average number n_i of photons during any single measurement. As a result, the Poisson noise associated with the input implies that $\sigma_i = (n_i)^{1/2}$. First suppose that the instrument produces no noise other than the quantum noise involved in converting photons to electrons. Then the average output number of events will be $n_o = Q\, n_i$, where Q is the quantum efficiency. For large enough n_o, the Poisson noise on the output will be $(n_o)^{1/2}$. Thus, for this simple case one finds $DQE = Q$.

However, an instrument in general introduces additional noise into the output. One way to view this is as an effective reduction in quantum efficiency. That is, the noise in the output equals the noise that would be produced by an otherwise-perfect instrument with a reduced quantum efficiency Q'. One sees that the maximum value of the *DQE* is Q. If the *DQE* is much less than any reasonable estimate of Q then the instrumental noise is dominant.

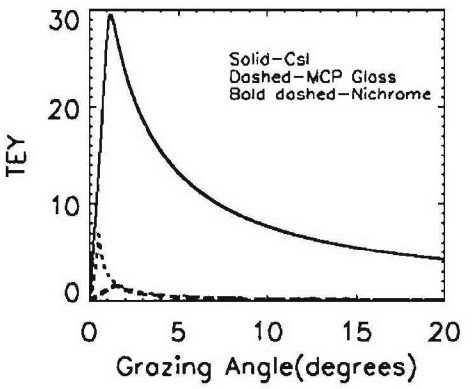

Figure 2. The total electron yield has a maximum at some small grazing angle. The actual number of photoelectrons released from a specific material at a specific angle is a Poisson distribution whose mean value is the *TEY*.

This picture is oversimplified for some complex instruments including MCPs. In the case of MCPs, the reason is that angle of incidence of the x-rays on the wall of a pore in the MCP varies greatly across the pore. For x-rays normally incident on an MCP with pores that are tilted by a bias angle θ, the grazing angle α at which the x-rays approach the surface of a pore varies from 0 to θ. Both the quantum efficiency Q (the fraction of photons producing photoelectrons) and the total electron yield *TEY* (the average number of secondary electrons produced when a single photon strikes the surface) vary strongly with this angle. What the *DQE* gives in this case is an effective quantum efficiency of an idealized instrument with a single angle of incidence and no other noise sources.

Figure 2 shows the variation in *TEY* with angle of incidence for three materials irradiated by Al Kα x-rays. The *TEY* was determined within the model discussed below but is also consistent with published values. At small grazing angles, an x-ray can stay near enough to the surface to release numerous photoelectrons. How efficient this is depends on the detailed properties of the material, discussed further in the context of the model below. One sees that the *TEY* has a different maximum value for various materials, and that it peaks at different angles for the different materials. (This relates to variations in the complex index of refraction and the range of the primary photoelectron.) Nichrome, which is shown as a bold dashed line, is the electrode material used to coat the MCP to allow application of the electric field used to accelerate the secondary electrons down the channels. A "bare" MCP actually in some sense has a Nichrome photocathode.

One implication of Eq. 1 is that various types of measurements will produce values of the *DQE* that are more or less sensitive to different noise sources. To use *DQE* to find the (average) quantum efficiency, one must operate the instrument in a regime where the quantum statistics of the source are the dominant contribution to the noise. For example, suppose the average quantum efficiency is 10%. If one were able to make measurements with 100 incident x-ray photons per measurement, then the average number of detected events would be 10 and the standard deviation would be 3.3 (or 33%). This would provide a reasonably accurate measurement of quantum efficiency. In addition, other sources of signal variation ("noise") even at the 10% level would not compromise this measurement. This reasoning led us to undertake the measurements of single-photoelectron events that have proven so informative.

On the other hand, suppose one makes a set of measurements each involving 10^5 incident x-ray photons in a system with an average quantum efficiency of 10%. In this case the standard deviation in the signal produced by photoelectron emission is 1%. If other sources of noise in the instrument amount to even a few percent of the signal, these will dominate and will determine the *DQE*. This type of measurement is most useful for characterization of system noise, of fixed-pattern noise reflecting average gain variations, and of spatial resolution and the modulation transfer function (MTF).

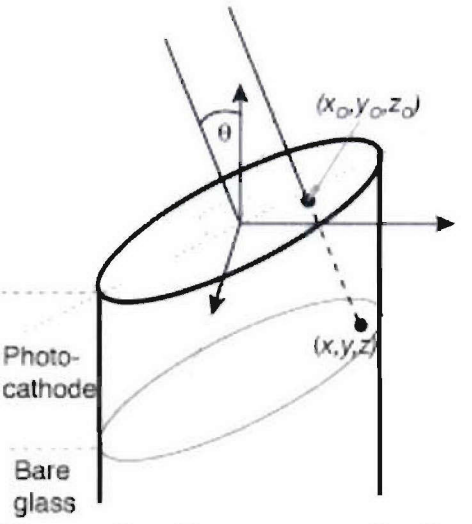

Figure 3. Geometry used for simulations. The MCP bias angle is θ. The channel mouth coordinates of an incident photon are (x_o,y_o,z_o). The coordinates of a photon strike on the channel wall are (x,y,z). Note that the channel mouth is an ellipse and photon path is normal to the ellipse plane

Working in the regime just described, we measured the *DQE* of a 2 inch CsI coated microchannel plate, using Pawley's method of sampling resolution elements from 100 individual exposures**[5]**. The MCP used for the DQE calculation is the same as that used to create Figure 1. However, for this measurement the MCP was operated at a voltage of 1050V with a CCD integration time of 3s, which yielded 47 photons per channel. In addition, the input and output measurements were averaged over a square of 50x50 CCD pixels(1 pixel = 9x9μm), so the mean of one square has less then 10% correlation with any of the neighboring squares' mean. Assuming the input noise is Poisson, the DQE is found to be 11%.

This understanding of *DQE* makes it clear that a complete analysis of MCP performance must include a more thorough analysis of the processes through which the MCP produces signal.

C. The Monte Carlo model and its results

To accomplish this more thorough analysis, Eric Harding developed a Monte Carlo model of MCP operation, written in IDL. We describe this model here. The code itself is provided as an appendix.

Fig. 3 illustrates how the geometry was defined for this calculation. Incident x-ray photons all approach the pore at the angle θ, which is the bias angle. Their location on the surface of the pore is chosen randomly. A geometric calculation then determines where they strike the wall of the pore, and at what grazing angle this occurs. It is worth noting that the actual value of the grazing angle is a very important parameter that can only be determined by a 3D model. Most models addressing MCP performance in the literature are 2D models. Such models will calculate the production of photoelectrons inaccurately.

In addition, the x-ray photon may strike the photocathode material or may strike bare glass, depending upon its location. As a result, these surfaces must be treated distinctly in the model. The interaction of the x-ray photon with the wall material produces some number of photoelectrons. The mean value of this number is the *TEY* shown in Fig. 2. The calculation of the *TEY* has several steps. First, one must calculate the complex index of refraction (n) for the material. This uses the energy-dependent, x-ray atomic scattering factors (f_1 and f_2) catalogued by Henke. One then finds the reflection coefficient for the x-rays using the Fresnel equation as written by Henke **[6]**. One also needs the linear x-ray absorption coefficient, μ, which can be obtained either from the NIST website or from the Henke paper, with slightly different results.

In addition, one needs some parameters that are not obtained from theory or tabulation but that are instead based on the extensive experimental work of Fraser and collaborators **[7,8]**. These include the escape probability for an a secondary electron at the surface, $P_s(0)$, the average energy required to create a secondary electron, ε, and the secondary electron escape length, L_s. These quantities and the above enter into an experimentally confirmed model by Fraser **[9]**, giving the *TEY*. In our Monte Carlo model, the actual number of photoelectrons produced in a given case is determined by randomly sampling the Poisson distribution that has the correct mean value (*TEY*). When the *TEY* is small, sampling the Poisson distribution will sometimes give zero secondary electrons. In this case the photon is considered not to have been detected. In the limit that $TEY << 1$, the Poisson distribution gives only 0 or 1 photons with any significant frequency. In this limit, $TEY = Q$.

To obtain a total value for the output produced by a single detected photon, labeled G above, the number of secondary photoelectrons must be multiplied by the amplification of each electron as it propagates down the channel. Assuming that the signal is not saturated, this amplification is described very well by modeling the channel as a discrete dynode electron multiplier, with the number of dynodes equal to the characteristic distance between electron bounces in the channel **[10,11]**. In such a model, the amplification is given by δ^{Nb}, where δ is the average secondary electron emission coefficient during amplification, and Nb is the number of bounces. The length of the channel determines the maximum value of Nb, but for any specific photoelectron, the value of Nb depends upon how far down this channel the photoelectron is produced. The geometric calculation described above determines this depth, and is used to set the gain for any specific group of photoelectrons.

The output of the model, for a calculation using 10^6 input photons, is shown in Fig. 4. In addition, Table 1 shows some key properties of this case. The left graph in Fig. 4 shows a distribution of events with three peaks. The high-signal events result from photons that strike CsI and have a large *TEY*. The group of events at a signal near 10^4 electrons is produced by the relatively few photons that interact near the peak of the *TEY* curve for glass as seen in Fig. 2. The bulk of the signal from the glass in produced by the larger number of photons that interact at angles up to the bias angle of 8 degrees. One can see in this graph that most of the events are produced in the glass; Table 1 reports that in

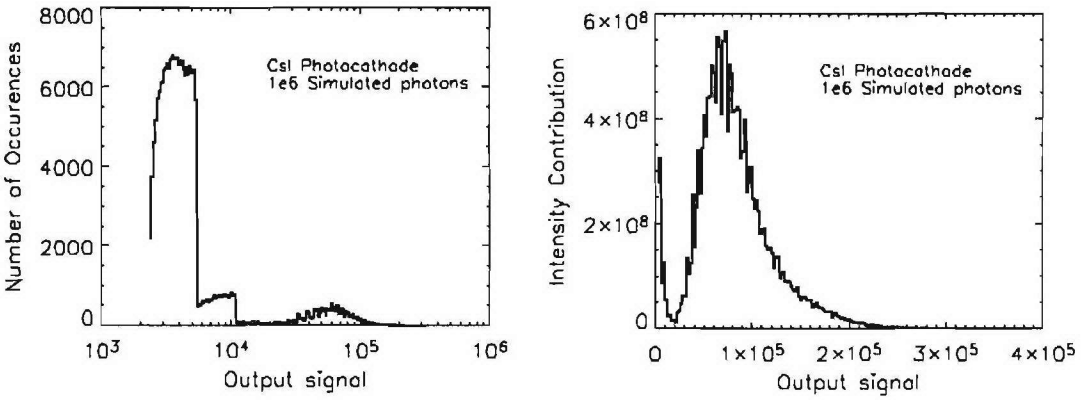

Figure 4. Results for an MCP with the following specifications: CsI photocathode coating ~1.5 channel diameters deep, 8 degree bias angle, V_{MCP} = 1150V, L/D = 60, 10μm diameter channels, 600μm thick MCP, radiated by 1.49keV x-rays. The figure on the left shows the number of events producing any given output signal. The figure on the right shows the intensity spectrum, obtained by multiplying the number of events times the signal in the left figure, and displayed on a linear scale. The steep jumps in the plot of the left are due to the sharp peak in the glass TEY curve as seen in Figure 2.

actuality 75% of the photons strike the glass. However, the quantum efficiency of these photons is only 33%. In contrast, 100% (to 3 digit accuracy) of the photons striking the CsI produce photoelectrons. As a result, equal numbers of events are produced by the photocathode and by the glass. This may not seem intuitive from the graph, because it is on a log scale.

The graph on the right in Fig. 4 shows the spectrum of signal intensity, on a linear scale so that relative area corresponds to fraction of total signal. Because the *TEY* of CsI is so much larger than that of the glass (see Fig. 2), 94% of the signal is produced by the CsI. For high-quality CsI under the conditions simulated here, one would expect the overall $\delta G/G$ to be ~ 43%. This is equivalent to a DQE of ~ 5% in a measurement having 100 photons incident on CsI inside pores per resolution element. The qualification "on CsI inside pores" is important. We have seen that 75% of the photons entering a pore do not strike the CsI. In addition, about half the photons strike the webbing between the pores. (Being normally incident, such photons have a lower TEY – 1.6 for Al Kα on CsI– but their potential contribution may not be negligible.) Overall, only 1/8 of the incident photons strike the photocathode material within the pores. Thus, it appears that the typical quantum efficiency discussed in the literature related to inertial fusion (of order 10%) represents near unity quantum efficiency for the small fraction of photons that

Table 1. Results of Monte Carlo simulation of MCP as described in the text

Surface struck	CsI	Glass
Total Intensity Contribution	94%	6%
Photon strikes	25%	75%
QE	100%	33%
δG / G	43%	167%

Table 2. Results of modeling a "bare" MCP

Surface Struck	Nichrome	MCP Glass
Strikes	82550	865058
Detected Events	24009	293109
Average flux(scaled)	36	27
Max flux(scaled)	611	855
Total flux(scaled)	4.96e8	3.96e9
Delta G / G	1.76	1.70
QE	29%	34%
Contribution to total signal	11.2%	88.8%

actually impact the photocathode material within the pores. The corresponding options for improving performance are discussed below.

For comparison, Table 2 shows the behavior of a "bare" channel plate, in which the electrode layer of nichrome provides a layer with a somewhat smaller average quantum efficiency than that of the glass. The value of δG/G for nichrome increases through the variation in the grazing angle α. A photon incident on the nichrome could have any grazing angle from 0 to the bias angle (8 degrees in our case). On the other hand, the photons striking the glass do not have access to all grazing angles, but experience a much larger variation of incident depth below the MCP surface. In the end, these effects balance and hence nichrome and glass have similar δG/G values.

Returning to the data of Fig. 1, we can compare the data we obtained with results from the simulation code, by modeling a case similar to that of the measurement. Figure 5 shows the results of such a simulation. Its properties are detailed in Table 3. In the experiment there were 0.016 photons per channel on average (so that multiple-photon events were negligible) and there were 84200 channels in the detected region, so that the number of photons incident on open channel area was 1360. In the simulation there were 1323 such photons. In the figure, the average flux from the simulation is scaled to match that of the data set. This accounts empirically for the conversion process from electrons leaving the MCP to counts in the CCD. One can see that the experiment produces fewer high-signal events than the model would expect. We attribute this to the fact that the coating on the plate used was old and had been worked with extensively. As a result, only a small fraction of the CsI photocathode was able to produce the anticipated level of signal. It is also possible that CsI even when new may perform differently than the model predicts, because the material is known to be somewhat "fluffy" so that the

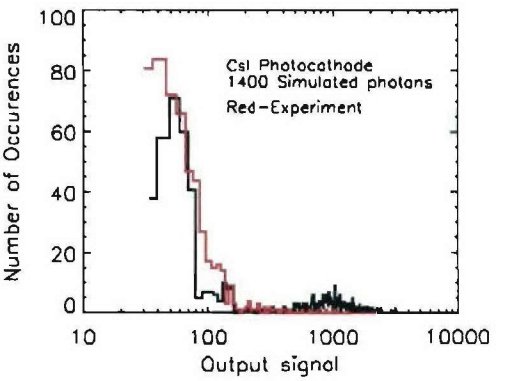

Figure 5. Comparison of data of Fig. 1 and output of simulation run with a similar total number of events.

local grazing angle may not equal the geometric value. In addition, the model does not yet include the loss of some photoelectrons out of the front surface of the pores, which will also reduce the signal produced by the CsI region. Even so, one would anticipate a larger group of high-signal photons from a CsI photocathode in good condition. One can see from Table 3 that the quantum efficiency and δG/G seen in the data are also consistent with the conclusion that most of the signal in this case comes from photons striking the glass.

We conclude that the approach of measuring the spectrum of single-photon events and comparing it to such a model is far more powerful in assessing the photocathode behavior and gain of an MCP than other approaches involving larger quantities of signal. (Other approaches are necessary to evaluate other properties including fixed pattern noise and MTF.) Correspondingly, we are working to improve the sensitivity of our detection system to see more of the spectrum and to make this practical at lower MCP operating voltage.

Table 3. Comparison of simulation and experiment

Material	CsI	MCP Glass	Experiment
Strikes	361	962	1360
Detected Events	361	331	535
Average flux(scaled)	1141	26	98 counts
Max flux(scaled)	3180	315	
δG / G	0.43	1.63	1.54
QE	100%	34%	39%
DQE	22%		10%
Material Flux/Total Flux	0.944	0.056	

The discussion above makes it clear that the signal strength and noise are influenced by three factors. These are the fraction of the incident photons that contribute meaningfully to the signal, the spectrum of total electron yield, and the spectrum of MCP gain. An effective framing camera design will optimize all three of these for any specific application. We suggest that this is feasible for high-value applications at NRL. This level of sophistication, for imaging applications, appears to us to be well beyond the previous state of the art for analog measurements using MCPs.

D. Resolution

The resolution of the framing is characterized by its modulation transfer function (MTF). The MTF is calculated by taking the absolute value of the Fast Fourier Transform of the linespread function of the framing camera. The linespread function was obtained by integrating over the image of a single channel event (appearing as a bright dot in Fig. 1), which is actually the point spread function (PSF) of the camera. The linespread function and corresponding MTF appear below in Figure 6.

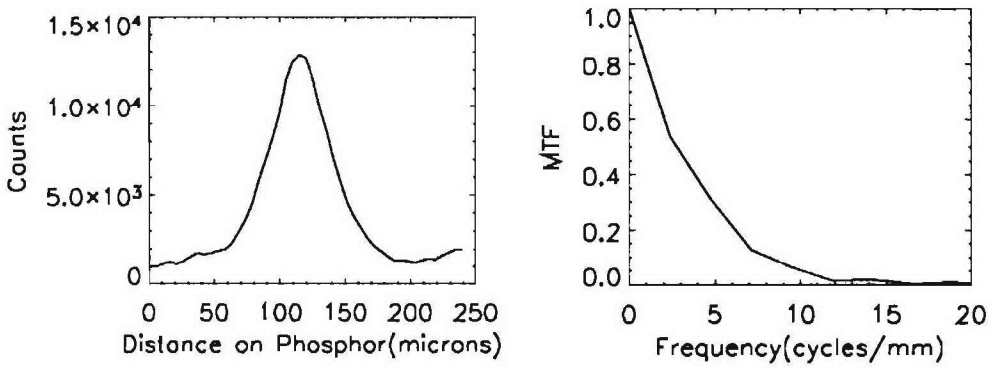

Figure 6. On the left is the linespread function determined by integrating over a single channel event. On the right is the corresponding MTF.

The point spread function has a FWHM of 50μm and a corresponding MTF of 4 lp/mm at 0.5. Pawley was able to achieve a better resolution of 10 lp/mm and increased sensitivity at lower spatial frequencies (larger Gaussian roll off in the MTF) by using a pulsed aluminized phosphor operated with a 250μm MCP-phosphor gap **[5]**. Pawley also pulsed the MCP voltage, which has been shown to decrease the transverse energy of an electron emitted from the rear of the MCP, and hence to improve the spatial resolution of the camera **[12]**. Thus, due the high MCP DC voltage (1150V) applied during collection of Fig. 1, we would expect a larger PSF FWHM compared to Pawley. Nevertheless, our framing camera MTF results are in similar to **[13]**, in which the camera shows no Gaussian roll off at low spatial frequencies due to the absence of an aluminized phosphor.

In the future we must develop the capability to pulse the MCP voltage, and incorporate a pulsed aluminized phosphor in order to demonstrate the highest possible framing camera resolution. This should also be done to demonstrate that any future novel camera design can be operated under conditions relevant to ICF.

E. Improvements to x-ray characterization system

We continue to make operational improvements to the x-ray system used for the measurements discussed above. The major improvement just completed was the purchase of a new CCD camera for detection. Our previous CCD cameras have been obtained second-hand from LLNL, and were not in optimum condition. In addition, LLNL has become much less reliable as a source of support and equipment. It was recently necessary to ask LLNL to recondition the module used to hold MCPs. This took a fairly long time. This is only one of several reasons, described below, why we intend to begin building MCP mounting hardware ourselves. We are now reworking the anode shield on our x-ray source to allow the installation of various filter assemblies. This will allow improved characterization of the x-ray source by K-edge spectroscopy.

We expect that the new CCD will have more sensitivity. We also purchased an inexpensive (< $1000) intensifier, and have tasked some undergraduates with measuring its gain and linearity. This provides another possible option for boosting sensitivity.

F. Participation at NRL

We have participated in activities at NRL during the past year. Eric Harding and Erika Roesler spent seven weeks at NRL during summer 2004. They worked with Yefim Aglitsky and Jim Weaver in diagnostic development. Their trip was scheduled with the intent that Eric would participate in some experiments on NIKE. Unfortunately, changes in the NIKE schedule precluded this.

References

1. O.L. Landen, et. al. Rev. Sci. Instrum., **75** (2004) 4037
2. K. McCammon, et. al, Ultrahigh Speed and High Speed Photograph, Photonics, and Videography '90, SPIE vol. **1346** p.398.
3. J.D. Wiedwald et. al. Ultrahigh Speed and High Speed Photograph, Photonics, and Videography '90, SPIE vol. **1346** p.449.
4. D.G Sterns, J.D. Wieldwald, B.M. Cook, R.L. Hanks, and O.L. Landen, Rev. Sci. Instrum. **60** (1989) 363
5. C.J. Pawley and A.V. Deniz, Rev. Sci. Instrum., **71** (2000)1286
6. B.L. Henke, Phys. Rev. A, **6** (1972) 94
7. G.W. Fraser, Nuc. Instrum. and Meth. A, **206** (1983) 265-279
8. G.J. Price and G.W. Fraser, Nuc. Instrum. and Meth. A, **474** (2001) 188-196
9. G.W. Fraser, Nuc. Instrum. and Meth. A, **206** (1983) 251-263
10. O.L. Landen, et. al., Rev. Sci. Instrum., **72** (2001) 709
11. E.H. Eberhardt, Applied Optics, **18** (1979) 1418
12. R.M. Estrella, S.W. Thomas, Ultrahigh Speed and High Speed Photograph, Photonics, and Videography '89, SPIE vol. **1155** p.367.
13. H.F. Robey, K.S. Budil, and B.A. Remington, Rev. Sci. Instrum. **68**, (1997) 792